# Theory of x-ray-absorption spectra in $PrO_2$ and some other rare-earth compounds

H. Ogasawara, A. Kotani, and K. Okada
*Department of Physics, Faculty of Science, Tohoku University, Sendai 980, Japan*

B. T. Thole
*Department of Chemical Physics, University of Groningen, Nijenborgh 16, 9747 AG Groningen, The Netherlands*
(Received 9 July 1990)

We analyze rare-earth $3d$-core x-ray-absorption spectra ($3d$ XAS) in $PrO_2$, as well as in $CeO_2$, using the impurity Anderson model. It is shown that the interplay between the atomic multiplet coupling and the solid-state hybridization between rare-earth $4f$ and oxygen $2p$ states is essential in determining the spectral shape. The calculated spectra are in fair agreement with experimental data which supports the theory that there is a strong mixing between $4f^1$ and $4f^2\underline{v}$ in the ground state of $PrO_2$, where $\underline{v}$ denotes a hole in the oxygen $2p$ valence band. A theoretical prediction of Pr $4d$ XAS of $PrO_2$ is also given. Because it contains much structure, experimental determination of this spectrum would be very valuable for the study of mixed-valence compounds.

## I. INTRODUCTION

Rare-earth dioxides, $CeO_2$, $PrO_2$, and $TbO_2$, are charge-transfer-type insulators with nominally "tetravalent" rare-earth ions. The electronic structure of these materials is characterized by a strong Coulomb interaction between $4f$ electrons, as well as by a covalency mixing between rare-earth $4f$ and oxygen $2p$ states. Core-level spectroscopy is a powerful tool in the study of electronic states of highly correlated systems,[1] and x-ray-absorption spectra (XAS) and x-ray-photoemission spectra (XPS) have been measured for these rare-earth dioxides.[2–11] As shown by Thole *et al.*,[12] the multiplet structure in XAS plays a role of "fingerprint" in examining the valence number of rare-earth ions, but the effect of a strong covalency mixing has not been well established. Due to the complexity of full multiplet calculations, the interpretation of the XAS multiplet structure in rare-earth dioxides was done intuitively, which produced quite a large amount of confusion.

Of these rare-earth dioxides, $CeO_2$ has been an object of the most extensive study by core-level spectroscopy both theoretically and experimentally.[13] Experimental data of $3d$ XPS, $3p$ XPS, $3d$ XAS, and $2p$ XAS of $CeO_2$ have been analyzed theoretically neglecting the multiplet structure using the impurity Anderson model. This showed that there is strong mixing between the $4f^0$ and $4f^1\underline{v}$ configurations ($\underline{v}$ denotes a hole in the O $2p$ valence band) in the ground state, with the average $4f$ electron number $n_f \sim 0.5$. However, the multiplet structure of $4d$ XAS in $CeO_2$ (Refs. 4 and 5) seemed, at first glance, to contradict the picture of a mixed-valence ground state mentioned above. Only very recently, Jo and Kotani,[14] Jo,[15] and the present authors[16] succeeded in carrying out the full calculations of $4d$ XAS, taking account of both the intra-atomic multiplet coupling and the interatomic covalency hybridization. It was shown that the multiplet structure in $4d$ XAS can also be well reproduced assuming a mixed-valence ground state.[14–16]

Improvement of our calculational methods now enables us to study $PrO_2$. Let us point out that there is a puzzling problem in the interpretation of $3d$ XAS of $PrO_2$. In Fig. 1, we show experimental data[9] of $3d$ XAS of $PrO_2$ and some Ce and La compounds. The $3d$ XAS of $PrO_2$ exhibits, in its $3d_{5/2}$ and $3d_{3/2}$ components, a main peak with some multiplet structures (indicated by arrows) and a satellite (indicated by "$s$"). Recently, a theoretical analysis of $3d$ XAS of $PrO_2$ was made by Bianconi *et al.*[11] using the impurity Anderson model without the multiplet-coupling effect. By this analysis, as well as by analysis of $2p$ XAS and $3d$ XPS, they concluded that the

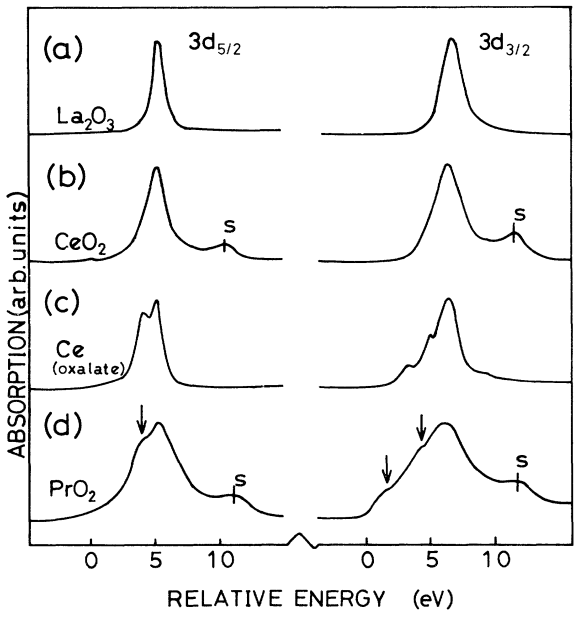


FIG. 1. Experimental $3d$ XAS for $La_2O_3$, $CeO_2$ Ce oxalate, and $PrO_2$ (after Ref. 9).

 

ground state of $PrO_2$ is a state with a strong mixing between the $4f^1$ and $4f^2\underline{v}$ configurations with $n_f \sim 1.6$, and that the main peak and the satellite correspond, respectively, to $3d^9 4f^3\underline{v}$ and $3d^9 4f^2$ final-state configurations, which are also strongly mixed. However, this interpretation contradicted the original one given by Karnatak *et al.*[6–9] who measured the experimental $3d$ XAS data. Using the multiplet structure as a fingerprint, they assigned the main peak of $PrO_2$ to the $3d^9 4f^2$ final state, instead of the $3d^9 4f^3\underline{v}$ state, because the multiplet structure of $PrO_2$ is similar to that of Ce oxalate, which is a typical $Ce^{3+}$ compound with a $3d^9 4f^2$ final state (see Fig. 1). Therefore, they concluded that $PrO_2$ contains only one localized $4f$ electron in the ground state. In order to explain the satellite, they introduced the concept of "extended $f$-type of states," and assigned the satellite to the transition of the $3d$ electron to these extended $f$ states. They emphasized that the situation in $CeO_2$ and $TbO_2$ is similar. As shown in Fig. 1, the spectral shape of the main peak of $CeO_2$ is similar to that of $La_2O_3$ but different from that of Ce oxalate. Therefore, they concluded that the main peak of $CeO_2$ corresponds to the $3d^9 4f^1$ final state as in the case of $La_2O_3$, while the satellite of $CeO_2$ originates from the transition to the extended $f$-type of states.

It is the purpose of the present paper to calculate the $3d$ XAS of $PrO_2$. The calculation can be carried out, as a straightforward extension of that in Ref. 16, by incorporating the interatomic hybridization into the intra-atomic multiplet spectra calculated by Cowan's programs.[17] We also analyze in more detail the multiplet structure in $3d$ XAS of $CeO_2$ as an extension of the theory by Jo and Kotani,[18] who first analyzed this spectrum and discussed the smearing out of the multiplet.

In Sec. II we describe our method of calculating $3d$ XAS of $PrO_2$. In Sec. III we show the calculated $3d$ XAS for $PrO_2$, as well as for $La^{3+}$, $CeO_2$, $Ce^{3+}$, and $Pr^{3+}$. Also, we give a theoretical prediction of $4d$ XAS in $PrO_2$. Concluding remarks are given in Sec. IV.

## II. METHOD OF CALCULATION

We use the impurity Anderson model, which consists of $4f$ and $3d$ states on a single Pr ion and a filled O $2p$ valence band. The Hamiltonian is essentially the same as that in Ref. 16, and given by

$$H = H_1 + H_2 , \tag{1}$$

where

$$\begin{aligned} H_1 = & \sum_{k,\nu} \varepsilon_k a^\dagger_{k\nu} a_{k\nu} + \varepsilon_f \sum_{\nu} a^\dagger_{f\nu} a_{f\nu} + \varepsilon_d \sum_{\xi} a^\dagger_{d\xi} a_{d\xi} \\ & + V/\sqrt{N} \sum_{k,\nu} (a^\dagger_{f\nu} a_{k\nu} + a^\dagger_{k\nu} a_{f\nu}) \\ & + U_{ff} \sum_{\nu > \nu'} a^\dagger_{f\nu} a_{f\nu} a^\dagger_{f\nu'} a_{f\nu'} \\ & - U_{fc} \sum_{\nu,\xi} a^\dagger_{f\nu} a_{f\nu} (1 - a^\dagger_{d\xi} a_{d\xi}) \end{aligned} \tag{2}$$

and $H_2$ describes the atomic Coulomb, exchange, and spin-orbit interactions, as given in Ref. 16. The Hamiltonian $H_1$ describes the usual impurity Anderson model without the multiplet-coupling effect. The energies $\varepsilon_k$, $\varepsilon_f$, and $\varepsilon_d$ represent the O $2p$ valence band, Pr $4f$ level, and Pr $3d$ level, respectively. We assume that $\varepsilon_k$ is given by $N$ discrete levels in the form

$$\varepsilon_k = \varepsilon_v - \frac{W}{2} + \frac{W}{N}(k - \tfrac{1}{2}), \quad k = 1, \ldots, N , \tag{3}$$

where $\varepsilon_v$ and $W$ are, respectively, the center and the width of the valence band. The index $\nu$ represents the spin and orbital degeneracies of the $f$ state, and $\xi$ those of the $3d$ state. The interactions, $V$, $U_{ff}$ and $-U_{fc}$, respectively, are the hybridization between $4f$ and valence-band states, the Coulomb interaction between $4f$ electrons, and the core-hole potential acting on the $4f$ electron.

We express the ground state $|g\rangle$ of $PrO_2$ in the following form:

$$\begin{aligned} |g\rangle = & C_1^g |d^{10} f^1; {}^2F_{5/2}\rangle \\ & + \sum_k \sum_{j=\frac{5}{2},\frac{7}{2}} \sum_{\alpha_J} C_2^g(k,j,\alpha_J) \\ & \times |d^{10} f^2(\alpha_J)\underline{v}_{kj}; J_{\text{tot}} = \tfrac{5}{2}\rangle , \end{aligned} \tag{4}$$

where $|d^{10} f^1; {}^2F_{5/2}\rangle$ is the Hund's-rule ground state ${}^2F_{5/2}$ of the $4f^1$ configuration, and

$$|d^{10} f^2(\alpha_J)\underline{v}_{kj}; J_{\text{tot}} = \tfrac{5}{2}\rangle$$

is the state with the total angular momentum $J_{\text{tot}} = \frac{5}{2}$, which is composed of the $4f^2$ configuration with symmetry $\alpha_J$ and the valence-band hole $\underline{v}$ with energy $\varepsilon_k$ and angular momentum $j (= \frac{5}{2}$ or $\frac{7}{2})$. Since the states $|d^{10} f^1; {}^2F_{5/2}\rangle$ and

$$|d^{10} f^2(\alpha_J)\underline{v}_{kj}; J_{\text{tot}} = \tfrac{5}{2}\rangle$$

are coupled to each other by the hybridization $V$, we obtain the state $|g\rangle$ and its energy $E_g$ by diagonalizing the Hamiltonian matrix with dimension $22N+1$.

In the final states $|i\rangle$ of dipole-allowed $3d$ XAS, the total angular momentum $J$ takes on the values $\frac{3}{2}$, $\frac{5}{2}$, and $\frac{7}{2}$. Each state $|i\rangle$ is given by a linear combination of $3d^9 4f^2$ and $3d^9 4f^3\underline{v}$ configurations in the form

$$\begin{aligned} |i\rangle = & \sum_{\alpha} C_2^i(\alpha_J) |d^9 f^2; \alpha_J\rangle \\ & + \sum_k \sum_{j=\frac{5}{2},\frac{7}{2}} \sum_{\alpha'_{J'}} C_3^i(k,j,\alpha'_{J'}) \\ & \times |d^9 f^3(\alpha'_{J'})\underline{v}_{kj}; J_{\text{tot}} = J\rangle , \end{aligned} \tag{5}$$

where $\alpha$ and $\alpha'$ are $LS$ terms. With the basis set of Eq. (5), the dimension of the Hamiltonian matrix is $(435N+15)$ for $J = \frac{3}{2}$, $(581N+19)$ for $J = \frac{5}{2}$, and $(656N+19)$ for $J = \frac{7}{2}$.

The Hamiltonian matrix elements both for the ground state and the final are obtained using Cowan's program,[17] and the matrix is diagonalized numerically to obtain $|g\rangle$, $E_g$, $|i\rangle$, and $E_i$, where $E_i$ is the energy of $|i\rangle$. Then the spectrum of $3d$ XAS is calculated in the form

$$F(\omega)=\sum_i |\langle i|T|g\rangle|^2 \frac{\Gamma/\pi}{(\omega+E_g-E_i)^2+\Gamma^2}\ , \qquad (6)$$

where $T$ is the dipole transition operator, $\omega$ is the photon energy, and $\Gamma$ represents the spectral broadening due to the lifetime of the core hole as well as the spectral resolution. The matrix element $\langle i|T|g\rangle$ is also obtained by Cowan's program.[17]

## III. CALCULATED RESULTS

The calculated $3d$ XAS for $PrO_2$ is shown in Fig. 2, where the line spectra are obtained in the limit of $\Gamma=0$ and the continuous spectra correspond to their convolution with a Lorentzian of width $\Gamma=0.7$ eV. The origin of the photon energy $\omega$ is fixed arbitrarily. The parameter values in the Hamiltonian $H_1$ are taken, in a manner consistent with previous analysis[11] of $3d$ XAS, $3d$ XPS, and $2p$ XAS, as $\varepsilon_f-\varepsilon_v=-10.0$ eV, $U_{ff}=10.5$ eV, $U_{fc}=13.0$ eV, $V=0.45$ eV, and $W=1.3$ eV. For Slater integrals and spin-orbit coupling constants included in the Hamiltonian $H_2$, we use the values of $Pr^{3+}$, which are given by Thole *et al.*[12] The value $N$ is taken to be $N=3$. With these parameters the average number of $4f$ electrons in the ground state is about 1.6, so that the system is a strongly mixed state between $4f^1$ and $4f^2\underline{v}$ configurations. From comparison between Fig. 1(d) and Fig. 2, the overall agreement between theoretical and experimental results is good. The theoretical calculation reproduces not only the satellite structure [indicated by "$s$" in Fig. 1(d)] but also the fine structure on the $3d_{3/2}$ main peak (indicated by arrows). There is, however, a discrepancy in the position of the shoulder on the $3d_{5/2}$ main peak; the shoulder is seen, in the experiment, on the lower-energy side of the main peak but on the higher-energy side in the calculation. In view of the success for $3d_{3/2}$ we still consider this calculation as supporting the mixed-valence picture.

In order to compare with the experimental data for $La_2O_3$, $CeO_2$, and Ce oxalate in Figs. 1(a)–1(c), we calculate the $3d$ XAS for a $La^{3+}$ ion, $CeO_2$, and a $Ce^{3+}$ ion, and show the result in Figs. 3(a)–3(c). The agreement between theoretical and experimental results is excellent. The calculated result for a $Pr^{3+}$ ion is also shown in Fig. 3(d). The results for $La^{3+}$, $Ce^{3+}$, and $Pr^{3+}$ are essentially the same as those given by Thole *et al.*,[12] while the result for $CeO_2$ corresponds to a finite-$W$ version of that by Jo and Kotani.[15] The parameter values (in the Hamiltonian $H_1$) used for the present calculation for $CeO_2$ are as follows: $\varepsilon_f-\varepsilon_v=1.5$ eV, $U_{ff}=12.5$ eV, $U_{fc}=13.5$ eV, $V=0.76$ eV, $\Gamma=0.7$ eV $W=1.3$ eV, and $N=6$. These values are consistent with those used in the previous analysis,[13,15,16] while a slight modification has been made to obtain better agreement with the experimental $3d$ XAS.

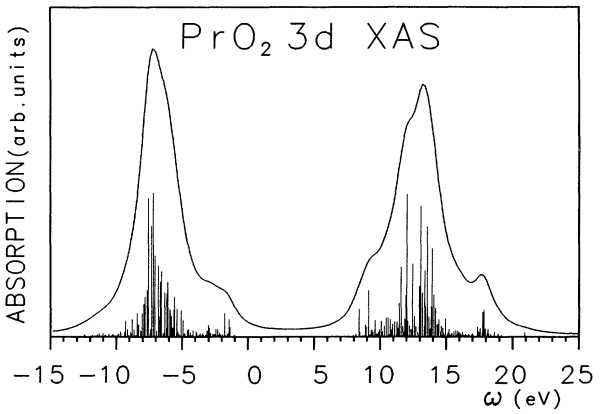


FIG. 2. Calculated $3d$ XAS for $PrO_2$.

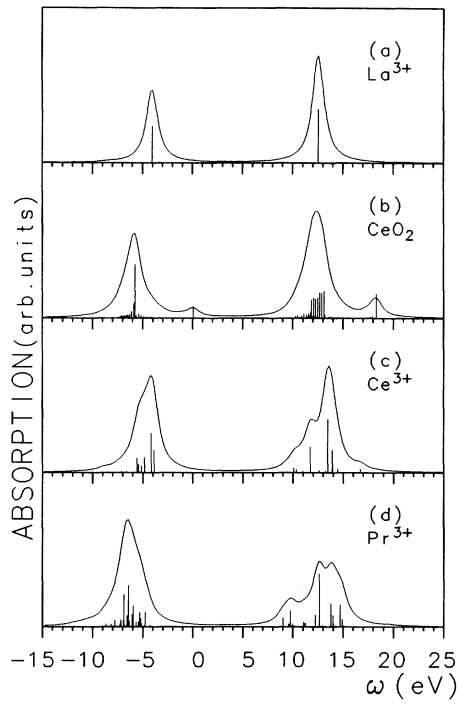


FIG. 3. Calculated $3d$ XAS for $La^{3+}$, $CeO_2$, $Ce^{3+}$, and $Pr^{3+}$.

Now we discuss the origin of the multiplet structure and the satellite of the $3d$ XAS for $PrO_2$. To this end, we calculate the spectrum by changing the hybridization strength *in the final state* $V_F$ with the other parameters fixed to the same values as those in Fig. 2. The result is shown in Fig. 4. When $V_F=0$ [Fig. 4(a)] the spectrum is a simple superposition of two absorption spectra corresponding to $3d^{10}4f^1\rightarrow 3d^9 4f^2$ (dotted curve) and $3d^{10}4f^2\underline{v}\rightarrow 3d^9 4f^3\underline{v}$ (dashed curve) transitions. The difference in the average energies between $3d^9 4f^2$ and $3d^9 4f^3\underline{v}$ final states

$$-\varepsilon_f+\varepsilon_v+U_{fc}-2U_{ff}(=2.0\text{ eV})$$

is smaller than the spread of the multiplet terms, so that the two spectra overlap strongly. Their intensity ratio is given by the relative weight of the $3d^{10}4f^1$ and $3d^{10}4f^2\underline{v}$ configurations in the ground state, which is about 0.4:0.6. It is to be noted that the multiplet structure of the $3d^{10}4f^1\rightarrow 3d^9 4f^2$ spectrum (dotted curve) is essentially the same as that of $Ce^{3+}$ in Fig. 3(c). However, the mul-

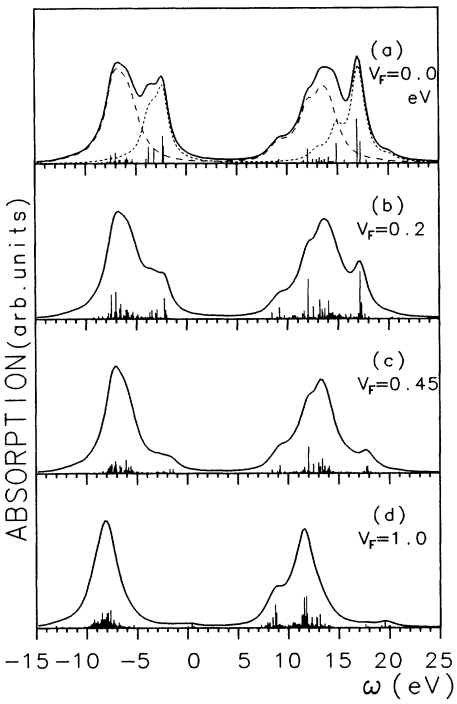


FIG. 4. Calculated $3d$ XAS for $PrO_2$ for the indicated values of the hybridization strength $V_F$ in the final state. The dotted and dashed curves are the $4f^1 \rightarrow 3d^9 4f^2$ and $4f^2\underline{v} \rightarrow 3d^9 4f^3\underline{v}$ components, respectively.

tiplet structure of the $3d^{10}4f^2\underline{v} \rightarrow 3d^9 4f^3\underline{v}$ spectrum (dashed curve) is considerably different from that of the $3d^{10}4f^2 \rightarrow 3d^9 4f^3$ spectrum of $Pr^{3+}$ in Fig. 3(d). This is because the initial state of the $3d^{10}4f^2\underline{v}$ configuration includes not only the Hund's-rule ground state $4f^2(^3H_4)$ of the $Pr^{3+}$ ion but also many other excited states $4f^2(\alpha_J)$ as given explicitly by the second term of the right-hand side of Eq. (4). Furthermore, the bandwidth $W$ of the valence-band hole $\underline{v}_{kj}$ causes a broadening of the spectrum.

When a small hybridization $V_F$ is introduced in the final state [Fig. 4(b)], two final-state configurations, $3d^9 4f^2$ and $3d^9 4f^3\underline{v}$, are mixed to form a bonding state (the lower-energy peak) and an antibonding state (the higher-energy peak). The intensity ratio of the lower-energy to higher-energy peaks increases with increasing $V_F$ because of the effect of the phase matching between ground and final states (note that the ground state is a bonding combination of $3d^{10}4f^1$ and $3d^{10}4f^2\underline{v}$). This effect is called the "hybridization-derived interference" in Ref. 18. The energy separation between the lower-energy and higher-energy peaks also increases with $V_F$. In Fig. 4(c) the value of $V_F$ is the same as that in Fig. 2, where the higher-energy peak is a weak satellite. It is interesting to note that the multiplet structure of the main peak is very similar to that of the dashed curve of Fig. 4(a). This means that the multiplet structure of $3d$ XAS for $PrO_2$ is mainly determined by the effect of the initial-state mixing, instead of the final-state mixing $V_F$, whereas the effect of $V_F$ is very important in determining the intensity ratio between the main peak and the satellite. When $V_F$ is further increased, the multiplet structure is also changed, as shown in Fig. 4(d).

The effect of $V_F$ is also studied in $3d$ XAS of $CeO_2$, and the result is shown in Fig. 5. Figure 5(a) is the case of $V_F=0$. The $4f^0 \rightarrow 3d^9 4f^1$ component is the same as the spectrum of $La^{3+}$ in Fig. 3(a), but the $4f^1\underline{v} \rightarrow 3d^9 4f^2\underline{v}$ component does not exhibit the multiplet structure which is seen in the spectrum of $Ce^{3+}$ in Fig. 3(c). The explicit form of the $3d^{10}4f^1\underline{v}$ state is

$$\sum_k \sum_{j=\frac{5}{2},\frac{7}{2}} C_1^g(k,j)|d^{10}f_j^1\underline{v}_{kj};J=0\rangle$$

as shown in Ref. 16, so that it contains both $4f^1(^2F_{5/2})$ and $4f^1(^2F_{7/2})$ components, while the initial state of $Ce^{3+}$ is the Hund's-rule ground state $4f^1(^2F_{5/2})$.[19] Furthermore, the energy distribution of the valence-band hole $\underline{v}_{kj}$ plays an essential role in smearing out the multiplet structure. Therefore, the dashed curve resembles the spectrum of $La^{3+}$ only accidentally. When $V_F$ is switched on, the intensity ratio of the lower-energy to higher-energy peaks increases and their energy separation becomes larger, as shown in Figs. 5(b)–5(d). In this way, the origin of the multiplet structure (or the origin of the smearing out of the multiplet structure), as well as the origin of the satellite, is very similar in $CeO_2$ and $PrO_2$.

In Fig. 6(a) we show a calculated result of Pr $4d$ XAS for $PrO_2$. The spectrum is divided into a giant absorption region (high-energy region) and a prethreshold region (low-energy region) which shows much structure. The procedure of the calculation and the parameter values are

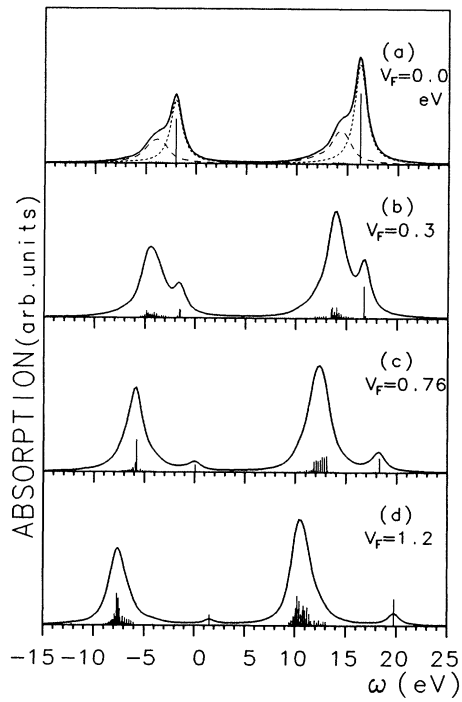


FIG. 5. Calculated $3d$ XAS for $CeO_2$ for the indicated values of the hybridization strength $V_F$ in the final state. The dotted and dashed curves are the $4f^0 \rightarrow 3d^9 4f^1$ and $4f^1\underline{v} \rightarrow 3d^9 4f^2\underline{v}$ components, respectively.

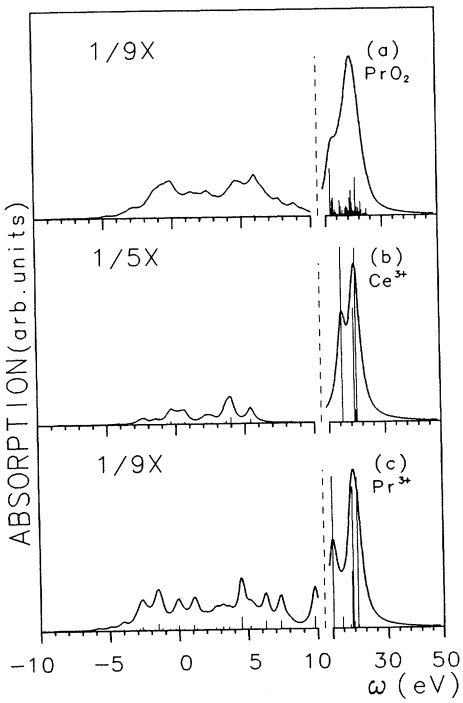


FIG. 6. Calculated $4d$ XAS for $PrO_2$, $Ce^{3+}$, and $Pr^{3+}$. The prethreshold region is amplified as indicated.

the same as those for $3d$ XAS, except that the parameter values associated with the core hole are changed. We take $U_{fc}(4d)=11.0$ eV, which is 80% of $U_{fc}(3d)$, and $\Gamma=2.0$ and 0.3 eV for the giant-absorption region and the prethreshold region, respectively. Slater integrals and spin-orbit coupling constants for final states are calculated by atomic Hartree-Fock programs with relativistic corrections.[17] Slater integrals $F^k(ff)$, $F^k(df)$, and $G^k(df)$ are reduced by 20, 25, and 33 %, respectively. [$F^2(ff)=9.98$ eV, $F^4(ff)=6.27$ eV, $F^6(ff)=4.51$ eV, $\zeta_f=0.106$ eV, $\zeta_d=1.375$ eV, $F^2(df)=10.6$ eV, $F^4(df)=6.77$ eV, $G^1(df)=11.06$ eV, $G^3(df)=6.92$ eV, and $G^5(df)=4.88$ eV.] In Figs. 6(b) and 6(c) we also show $4d$ XAS calculated for $Ce^{3+}$ (which corresponds to $Pr^{4+}$) and $Pr^{3+}$ atoms. The important feature is that the $4d$ XAS of $PrO_2$ is different from those of $Ce^{3+}$ and $Pr^{3+}$. Therefore, when it becomes available, $4d$ XAS can be used as "fingerprint" to confirm our mixed-valence picture for $PrO_2$.

## IV. CONCLUDING REMARKS

We have analyzed $3d$ XAS of $PrO_2$ and $CeO_2$ with the impurity Anderson model including the intra-atomic multiplet effect. We have shown that the ground state of these materials is of mixed-valence nature, but the fine multiplet structure of the main peak looks like the tetravalent one because the effect of the initial state hybridization mixes the trivalent component $4d^{10}4f^n\underline{v}$ ($n=1$ and 2 for $CeO_2$ and $PrO_2$) with excited states and changes its spectral shape into the tetravalence-like one accidentally. Especially in $CeO_2$, the effect of the finite-energy width of $\underline{v}$ is important in smearing out the multiplet structure of the trivalent component. This effect is less important in $PrO_2$ because of the smaller hybridization strength. The effect of the final-state hybridization is important in determining the intensity ratio between the main peak and the satellite, but the spectral shape of the main peak remains almost unchanged from that for $V_F=0$.

For $CeO_2$, Jo and Kotani[18] carried out a similar calculation in the limit of vanishing valence-band width. They did not study the effects of the initial-state hybridization and the final-state hybridization separately, and emphasized the importance of "hybridization-derived interference" (the interference between initial-state and final-state hybridizations) in the smearing out of the trivalent multiplet structure of the main peak. In the present calculation we have taken into account the finite width of the valence band and pointed out the importance of the initial-state hybridization in smearing out the multiplet structure.

For $PrO_2$, the main structures of the multiplet and the satellite are satisfactorily reproduced in the present analysis, but there remains a small discrepancy between theoretical and experimental spectral shapes of the shoulder of the $3d_{5/2}$ main peak. Considering the success in reproducing most of the other structures, as well as the success in the analysis for $CeO_2$ which is a material quite similar to $PrO_2$, we do not think that the above discrepancy seriously challenges our mixed-valence picture for $PrO_2$. In any case, further study will be necessary on the shoulder structure both theoretically and experimentally. In order to confirm more definitely the mixed-valence picture for $PrO_2$, the experimental observation of $4d$ XAS is highly desirable.

Finally, it should be mentioned that there has been a long-standing controversy of whether or not $CeO_2$ and $PrO_2$ are mixed-valence systems. These materials were traditionally considered to be purely tetravalent systems with $4f^0$ ($CeO_2$) and $4f^1$ ($PrO_2$) configurations in the ground state. From quantitative analyses of core-level spectroscopic data, however, the mixed-valence picture was proposed (see Ref. 13 for more details of experimental and theoretical studies). As mentioned in Sec. I, most of the core-level data were well interpreted by the mixed-valence picture, but only the multiplet structures in $3d$ and $4d$ XAS seemed to support the tetravalence picture. The present paper, together with a series of related papers,[14–16,18] has shown from more extended quantitative calculations that the interpretation of the $PrO_2$ and $CeO_2$ spectra, especially of their multiplet structures, can be achieved with a unified picture of the mixed-valence ground state, to clear up the controversial points in previous interpretive works.

## ACKNOWLEDGMENTS

This work is partially supported by a Material Function Grant from International Joint Research Project from the New Energy and Industrial Technology Development Organization (NEDO), the International Joint Research Project from the Japan Society for the Promotion of Science (JSPS), and a Grant-in-Aid for Scientific Research from the Ministry of Education, Science and Culture in Japan. We would like to thank Professor G. A. Sawatzky for this support in carrying forward these International Joint Research Projects.

[1]See, for instance, *Core-Level Spectroscopy in Condensed Systems,* edited by J. Kanamori and A. Kotani (Springer, Heidelberg, 1988).

[2]E. Wuilloud, B. Delley, W.-D. Schneider, and Y. Baer, Phys. Rev. Lett. **53**, 202 (1984).

[3]G. Kaindl, G. Kalkowski, W. D. Brewer, E. V. Sampathkumaran, F. Holtzbert, and A. Schach v. Wittenau, J. Magn. Magn. Mater. **47-48**, 181 (1985).

[4]T. Hanyu, H. Ishii, M. Yanagihara, T. Kamada, T. Miyahara, H. Kato, K. Naito, S. Suzuki, and T. Ishii, Solid State Commun. **56**, 381 (1985).

[5]G. Kalkowski, C. Laubschat, W. B. Brewer, E. V. Sampathkumaran, M. Domke, and G. Kaindl, Phys. Rev. B **32**, 2717 (1985).

[6]R. C. Karnatak, M. Gasgnier, H. Dexpert, J. M. Esteva, P. E. Caro, and L. Albert, J. Less-Common Met. **110**, 377 (1985).

[7]J. M. Esteva and R. C. Karnatak, in *Giant Resonances in Atoms, Molecules and Solids,* edited by J. P. Connerade, J. M. Esteva, and R. C. Karnatak (Plenum, New York, 1987), p. 361.

[8]R. C. Karnatak, J. M. Esteva, H. Dexpert, M. Gasgnier, P. E. Caro, and L. Albert, J. Magn. Magn. Mater. **63&64**, 518 (1987).

[9]R. C. Karnatak, J.-M. Esteva, H. Dexpert, M. Gasgnier, P. E. Caro, and L. Albert, Phys. Rev. B **36**, 1745 (1987).

[10]A. Bianconi, I. Davoli, S. Della Longa, J. Garcia, K. B. Garg, A. Kotani, and A. Marcelli, in *Theoretical and Experimental Aspects of Valence Fluctuations and Heavy Fermions,* edited by L. C. Gupta and S. K. Malik (Plenum, New York, 1987), p. 243.

[11]A. Bianconi, A. Kotani, K. Okada, R. Giorgi, A. Gargano, A. Marcelli, and T. Miyahara, Phys. Rev. B **38**, 3433 (1988).

[12]B. T. Thole, G. van der Laan, J. C. Fuggle, G. A. Sawatzkey, R. C. Karnatak, and J.-M. Esteva, Phys. Rev. B **32**, 5107 (1985).

[13]See, for a review paper, A. Kotani, T. Jo, and J. C. Parlebas, Adv. Phys. **37**, 37 (1988).

[14]T. Jo, and A. Kotani, Phys. Rev. B **38**, 830 (1988).

[15]T. Jo, J. Phys. Soc. Jpn. **58**, 1452 (1989).

[16]A. Kotani, H. Ogasawara, K. Okada, B. T. Thole, and G. A. Sawatzky, Phys. Rev. B **40**, 65 (1989).

[17]R. D. Cowan, *The Theory of Atomic Structure and Spectra* (University of California Press, Berkeley, 1981).

[18]T. Jo and A. Kotani, J. Phys. Soc. Jpn. **57**, 2288 (1988).

[19]G. van der Laan, B. T. Thole, G. A. Sawatzky, J. C. Fuggle, R. Karnatak, J.-M. Esteva, and B. Lengeler, J. Phys. C **19**, 817 (1986).